Effects of antimony and ion damage on carrier localization in molecular-beam-epitaxy-grown GaInNAs

S. R. Bank,[a] M. A. Wistey, H. B. Yuen, V. Lordi, V. F. Gambin, and J. S. Harris, Jr.
Solid State and Photonics Laboratory, Stanford University, Stanford, California 94305

(Received 27 October 2004; accepted 17 January 2005; published 13 June 2005)

We investigate the effects of both nonradiative recombination centers and compositional inhomogeneity on low-temperature localization in GaInNAs quantum wells. With the introduction of antimony and a reduction of nitrogen plasma-related damage during growth, localization energies as low as 2.5 meV are reported for single quantum well samples with room temperature emission at 1.5 μm. Moreover, low-temperature photoluminescence spectra revealed a broad, sub-band-gap luminescence peak that is ascribed to plasma-related defects. Deviation from the Varshni dependence of the band gap below 50 K was also observed and attributed to compositional inhomogeneity that localizes emission; however, no "S shape" was observed. Localization effects were found to depend upon the excitation density. © *2005 American Vacuum Society.*
[DOI: 10.1116/1.1878995]

I. INTRODUCTION

Pioneering work by Kondow and co-workers showed the emission wavelength of GaAs-based structures could be extended to the 1.3 μm regime with the introduction of nitrogen into InGaAs.[1] The low equilibrium solubility of nitrogen in InGaAs(Sb) gives rise to the metastability of GaInNAs(Sb), complicating the growth. By appropriately controlling the molecular-beam epitaxy (MBE) growth process, the laser emission wavelength has been extended to 1.59 μm and low-threshold dilute nitride lasers in the 1.5–1.53 μm regime have been demonstrated.[2–6] Low growth temperatures and the inherent metastability of the material cause both high defect densities and compositional inhomogeneity. Together, these effects can cause anomalous variation in the temperature dependence of the measured band gap. Such localization effects are evident in temperature-dependent photoluminescence (PL), photoreflectance, and absorption. Typically occurring below 150 K, significant localization has been reported in GaInNAs alloys by several groups and, in some cases, manifests itself as an "S shape" in the band gap shift versus temperature $\Delta E_g(T)$ — a redshift-blueshift-redshift with increasing temperature.[7–9] Pinault and Tournie[8] found that material quality, specifically the number of nonradiative centers, is directly related to the severity of localization and the temperature at which it occurs. With improvements in material quality, such as those reported by Misiewicz and collaborators, the S shape has recently been suppressed for nitrogen content <4%.[9] Some degree of localization still remains at low temperatures (<70 K), as evidenced by a saturation of $\Delta E_g(T)$ and divergence from the Varshni equation. To quantify this effect, Misiewicz and co-workers adopted the energy separation between the Varshni fit and the measured data at 10 K, as proposed originally by Pinault and Tournie.[8] This low-temperature localization energy was found to be directly proportional to the nitrogen mole fraction for high-quality GaInNAs, at 2.36 meV/%N, from their data.[9]

Using the 10 K localization energy as a metric, we show reductions in the localization from both the addition of antimony into GaInNAs and the use of ion deflection plates during MBE growth. The addition of antimony was found to reduce the localization energy, as expected from work on surfactant-mediated growth. No S shape was observed, even for pump power densities as low as 1 W/cm^2. In optimally prepared structures, localization energies as low as 2.5 meV were observed, despite the high nitrogen content of 2.7%, for GaInNAsSb quantum wells (QW) with room temperature emission at ~1.5 μm.

II. EXPERIMENTAL METHODS

Single QW samples were grown by solid-source MBE, as described previously.[2,5] To modulate the ion damage during growth, deflection plates were installed at the output of the SVT Associates rf nitrogen plasma cell. For samples grown without deflection plates, both plates were grounded. When deflection plates were employed, they were biased to −40 V and ground. This voltage combination produced the minimum total current from remote Langmuir probe measurements.[10] This is likely nonoptimal, based on more recent work, and somewhat higher positive deflection voltages (≳60 V and ground) will likely show added improvement. Annealing was performed *ex situ* at 740 °C for 1 min, under a nitrogen ambient, in a rapid thermal annealing furnace. Arsenic out-diffusion was minimized by a GaAs proximity cap. As a frame of reference for the low-temperature measurements, peak PL emission at room temperature was improved by approximately twofold due to the addition of antimony, threefold due to annealing, and fivefold due to deflection plates.

For temperature-dependent PL measurements, samples were mounted strain-free on the cold finger of a cryostat with minimum temperature of ~10 K. The luminescence was collected and collimated by an $f/1$ lens and focused into an $f/4$

[a]Electronic mail: sbank@stanfordalumni.org

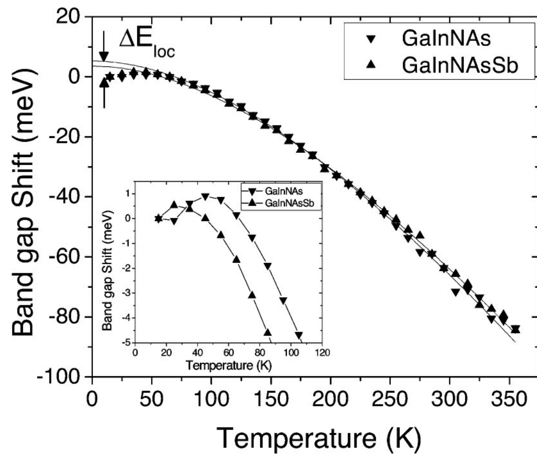

FIG. 1. Band gap shift with temperature for GaInNAs and GaInNAsSb QWs with room temperature emission ~1.3 μm. The localization was reduced by the introduction of antimony to the QW, due to improvements in optical quality and compositional homogeneity. Inset shows a close-up view of the band gap shift below 100 K. To clearly resolve the low-temperature behavior, peaks were determined by the line shape fitting described in Sec. V. The uncertainty in the peak location is ±0.1 meV for the inset. A decrease in both the severity and onset temperature of the low-temperature blueshift is clearly observed for the GaInNAsSb sample.

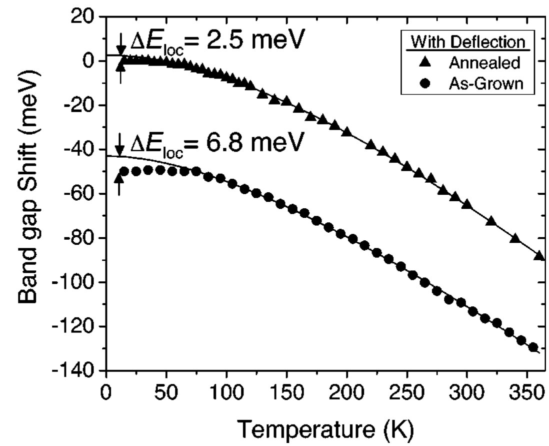

FIG. 2. Band gap shift with temperature and Varshni fits for a 1.5 μm GaInNAsSb QW grown with deflection plates before and after annealing at 740 °C for 1 min. Plots have been offset by 50 meV for clarity.

0.3 m spectrometer, with wavelength resolution set to 1 nm. The signal was detected with an uncooled InGaAs photodiode and a lock-in amplifier. Excitation was achieved using a multiline Ar^+ laser, with power densities as low as 1 W/cm^2, below the excitation density required to observe localization effects (typically 5–100 W/cm^2). Spectra were calibrated for the spectral response of the measurement system. Taking the wavelength with the highest signal as the PL peak was sufficient to accurately determine the localization energy. However, to adequately resolve small shifts in the PL peak at low temperatures, it was necessary to determine the PL maximum more precisely using the fitting procedure discussed in Sec. V. For the inset of Fig. 1, the maximum of the total fitted luminescence lineshape was taken as the PL peak. With this approach, the PL peak was determined to within ±0.1 nm, from the variance-covariance matrix, accounting for wavelength resolution and system in the data.

III. LOCALIZATION MEASUREMENTS

Figure 1 compares the temperature dependence of the band gap shift $\Delta E_g(T)$ for a single $Ga_{0.70}In_{0.30}N_{0.016}As_{0.984}$ QW (~1.3 μm emission at room temperature) and a single $Ga_{0.69}In_{0.31}N_{0.016}As_{0.964}Sb_{0.024}$ QW (~1.38 μm emission at room temperature). Deflection plates were not employed during growth. The localization energies were 4.5 and 3.4 meV for the as-grown GaInNAs and GaInNAsSb samples, respectively. Without antimony, the localization was larger than that found by Misiewicz and co-workers; with antimony, however, the localization energy was less than expected from their data.

Localization was further reduced through the use of ion deflection plates and annealing. Figure 2 shows $\Delta E_g(T)$ for a single $Ga_{0.63}In_{0.37}N_{0.027}As_{0.958}Sb_{0.015}$ QW sample grown with deflection plates, as-grown and after anneal at 740 °C for 1 min. The localization energy was found to be 2.5 meV after annealing, more than twofold lower than predicted by the model for a sample with 2.7% nitrogen. Table I summarizes the localization energies for samples grown with and without deflection plates, before and after annealing. As-grown samples showed a localization of ~6–7 meV, similar to the predicted nitrogen dependence, but somewhat lower with deflection plates. The localization energy was also reduced with anneal. Reduced localization with both annealing and deflection plates supports the conclusion that the defect density plays a key role in the localization behavior. Moreover, localization may not be an inherent material property. It is noted that reasonable qualitative fitting could be obtained for localization energies ±~1 meV of the quoted values, but the uncertainty from the variance-covariance matrix of the least-squares fit was ±0.3 meV.

IV. EXCITATION DENSITY

Localization effects were also seen to be excitation density dependent. Figure 3 plots the band gap with temperature for the as-grown $Ga_{0.70}In_{0.30}N_{0.016}As_{0.984}$ QW (room-temperature emission ~1.3 μm) of Sec. III, for excitation

TABLE I. Localization energies for 1.5 μm GaInNAsSb samples with and without deflection plates, before and after anneal. Improvements in optical quality through the use of deflection plates and anneal reduced the localization energy.

Sample	ΔE_{loc} at 10 K (meV)
As-grown No deflection plates	7.3±0.3
As-grown With deflection plates	6.8±0.3
Annealed No deflection plates	5.3±0.3
Annealed With deflection plates	2.5±0.3

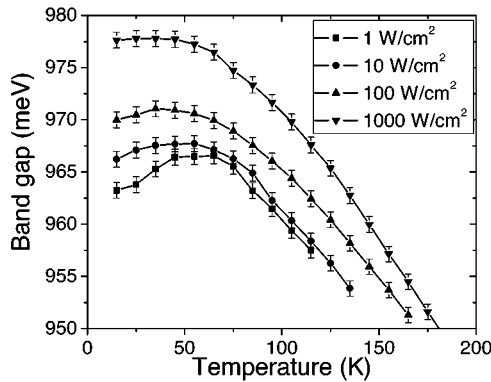

FIG. 3. Band gap shift with temperature for the 1.3 μm GaInNAs QW of Fig. 1 for several excitation densities. The degree of low-temperature blueshift and the localization energy were strongly affected by the excitation density. Error bars due to the spectrometer resolution of ±1 nm (approximately ±0.74 meV) are shown.

densities from 1 to 1000 W/cm^2. The most striking feature is an initial blueshift in the peak emission with increasing temperature, under low excitation (e.g., 1 W/cm^2). This is quite similar in appearance, although lower in magnitude, to the blueshift (delocalization) portion of the S-shape behavior. The underlying cause is likely compositional inhomogeneity that localizes carriers at potential fluctuations at low temperature. Such a mechanism is hidden under strong excitation by carrier filling, or at high temperatures through population statistics. Additionally, the entire $\Delta E_g(T)$ curve blueshifted with increasing excitation density, due to the higher carrier densities created in the QW. It is also noted that the degree of blueshift with excitation density (~14 meV at 15 K) was significantly greater than the value of the localization energy (4.5 meV). The localization energy should, therefore, not necessarily be viewed as an exact measure of the inhomogeneity in the conduction band, but rather as a figure of merit to gauge the degree of localization.

Excitation density also affected the fitted localization energy and the Varshni parameters. The localization energy decreased with increasing excitation density, as shown in Fig. 4(a). Likewise, the Varshni parameters approached typical III-V values at elevated excitation densities, shown in Fig. 4(b).

V. LINE SHAPE ANALYSIS

In an attempt to correlate the localization energy with the defect density, peak fitting was undertaken using the free exciton and interband (free-carrier) line shapes defined by Christen and Bimberg.[11] Virtually identical results were found using the line shapes defined by Colocci and co-workers[12] that were derived from somewhat different considerations. Lifetime broadening was assumed to be negligible compared to statistical broadening, a valid assumption for the dilute nitrides. It was not necessary to account for the contribution of $\boldsymbol{k} \neq 0$ recombination or other sources of asymmetry to accurately match the data; the resulting exciton line shape was Gaussian. A Gaussian line shape is expected in this material because of the high electron effective

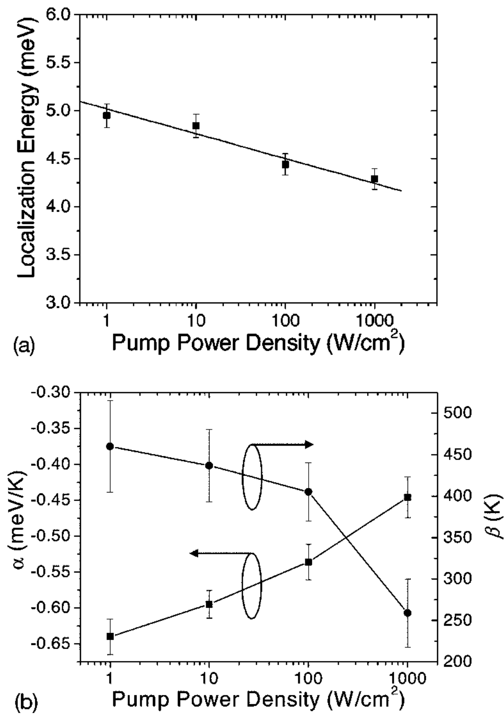

FIG. 4. Plots of (a) the localization energy and (b) the Varshni parameters, as functions of the excitation density, for the GaInNAs QW of Fig. 3.

mass, large exciton radius, and intrinsic lattice defects that lead to strong exciton-phonon coupling, even at relatively low temperatures.[13] A significantly weaker third peak was required to fit the low-energy portion of the spectrum for temperatures <75 K. A Gaussian line shape was assumed for this peak. The inset of Fig. 5 shows a PL spectrum and lineshape fit of the 1.3 μm as-grown $Ga_{0.70}In_{0.30}N_{0.016}As_{0.984}$ QW at 15 K, under 100 W/cm^2 excitation. Excellent fitting of the spectrum was accomplished with the above mentioned line shapes. Substantially poorer fitting was obtained using a

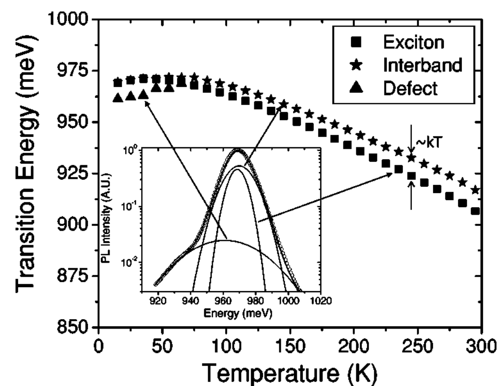

FIG. 5. Shift with temperature of peaks observed in the PL line shape for the GaInNAs QW of Fig. 1 under 100 W/cm^2 excitation density. Inset shows an example spectrum at 15 K. Three peaks are visible. The two highest energy peaks are attributed to excitonic and interband recombination, while the broad low-energy peak is attributed to defects. The defect-related peak energy appeared constant with temperature, to within the resolution of the fitting.

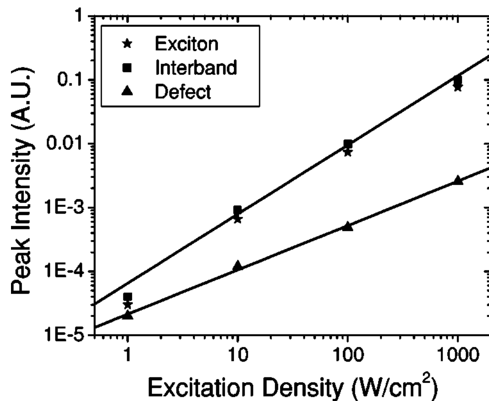

FIG. 6. Peak intensity with excitation density of the excitonic, interband, and defect peaks at 15 K. The defect level luminescence became comparable to the main transition at low excitation densities, consistent with the expected behavior of a defect level.

Lorentzian exciton line shape, confirming the assumption that statistical broadening is a significantly larger effect than lifetime broadening.

Figure 5 shows the temperature evolution of the three peaks. As expected, the exciton and interband peaks track one another with temperature. The low-energy peak is tentatively attributed to plasma-related defects as it is quite broad and did not shift significantly with temperature, as shown in Fig. 5. Moreover, the integrated intensity of this peak was reduced significantly by the use of deflection plates, but not with the introduction of antimony (not shown). The defect luminescence was also observed to become a more significant component of the PL spectrum at reduced excitation densities, as shown in Fig. 6. The peak intensities are expected to be comparable at excitation densities $\sim 0.1\ \mathrm{W/cm^2}$.

VI. CONCLUSION

We have investigated the dependence of localization effects on material quality and compositional homogeneity. The localization energy was reduced from 4.5 to 3.4 meV with the addition of antimony. We observed a decrease in the degree of low-temperature blueshift (at fixed excitation density) when compositional homogeneity was improved through the addition of antimony. Additionally, the temperature at which the blueshift began was decreased with antimony. The degree of blueshift with temperature was seen to depend upon the excitation density, indicating a correlation with compositional homogeneity—the magnitude of the observed localization effects were dependent upon the excitation density.

A relation between nonradiative recombination and the localization energy was also established. Reduced localization was observed with decreased ion damage during QW growth. A significant plasma-related defect peak was identified at low temperatures through line shape analysis. With significantly higher defect density, this peak could be responsible for the S-shape behavior that has been observed in GaInNAs, but further investigation is required. Postgrowth annealing, which likely improved both compositional homogeneity and nonradiative recombination, also reduced localization effects to as low as 2.5 meV for nitrogen content of $\sim 2.7\%$. This analysis validates localization measurements as a valuable method for examining both the compositional homogeneity and optical quality of dilute nitride QW layers.

ACKNOWLEDGMENT

The authors benefited from discussions with R. Kudrawiec of Wroclaw University, Poland and A.R. Kovsh of NL Nanosemiconductor GmbH. This work was supported under DARPA and ARO contracts, DAAD17-02-C-0101, and DAAD199-02-1-0184, MARCO Interconnect Focus Center contract, B-12-M06-S1 and the Stanford Network Research Center (SNRC). V. Lordi was supported by the Hertz Foundation.

[1] M. Kondow, T. Kitatani, S. Nakatsuka, M. C. Larson, K. Nakahara, Y. Yazawa, M. Okai, and K. Uomi, IEEE J. Sel. Top. Quantum Electron. **3**, 719 (1997).
[2] V. Gambin, W. Ha, M. A. Wistey, H. Yuen, S. R. Bank, S. M. Kim, and J. S. Harris Jr., IEEE J. Sel. Top. Quantum Electron. **8**, 795 (2002).
[3] M. Fischer, M. Reinhardt, and A. Forchel, Electron. Lett. **36**, 1208 (2000).
[4] L. H. Li, V. Sallet, G. Patriarche, L. Largeau, S. Bouchoule, L. Travers, and J. C. Harmand, Appl. Phys. Lett. **83**, 1298 (2003).
[5] S. R. Bank, M. A. Wistey, L. L. Goddard, H. B. Yuen, V. Lordi, and J. S. Harris Jr., IEEE J. Quantum Electron. **40**, 6, 656 (2004).
[6] G. Jaschke, R. Averbeck, L. Geelhaar, and H. Riechert, J. Cryst. Growth (in press).
[7] A. Kaschner, T. Luttgert, H. Born, A. Hoffman, A. Yu Egorov, and H. Riechert, Appl. Phys. Lett. **78**, 1391 (2001).
[8] M. A. Pinault and E. Tournie, Appl. Phys. Lett. **78**, 1562 (2001).
[9] J. Misiewicz, P. Sitarek, K. Ryczko, R. Kudrawiec, A. Fischer, M. Reinhardt, and A. Forchel, Microelectron. J. **34**, 737 (2003).
[10] M. A. Wistey, S. R. Bank, H. B. Yuen, H. P. Bae, and J. S. Harris Jr., J. Cryst. Growth (in press).
[11] J. Christen and D. Bimberg, Phys. Rev. B **42**, 7213 (1990).
[12] M. Colocci, M. Gurioli, and A. Vinattieri, J. Appl. Phys. **68**, 1809 (1990).
[13] Y. Toyozawa, Prog. Theor. Phys. **20**, 53 (1958).